Polymer Micromachined Transmission for Insect–Inspired Flapping Wing Nano Air Vehicles*

Daisuke Ishihara, Sunao Murakami, *Member, IEEE*, Naoto Ohira, Jyunpei Ueo, Masakatsu Takagi, Kohei Urakawa, and Tomoyoshi Horie

Abstract— **This paper presents a polymer micromachined transmission from small translational displacement to large rotational displacement, which has the potential for further miniaturizing a variety of micro robot applications such as insect-inspired flapping wing nano air vehicles (FWNAVs). Innovative claims include (1) the transmission mechanism using a geometrically nonlinear bending, (2) the microfabrication process consisting of only the standard steps such as the deposition, the photolithography, the curing, and the release without any post-assembling, and (3) the stroke angle of about 40° without any dynamic effect.**

I. Introduction

Insect-inspired flapping wing nano air vehicles (FWNAVs) [1, 2] have received much attention in recent years as a potent approach for miniaturizing unmanned air vehicles. Since minimum flying insect is about 1mm in its size scale, flapping wing nano air vehicles (FWNAVs) can be minimized into the size from the mechanical view point [3]. For their construction, one priority is to obtain the wing's flapping motion with the large stroke angle, since the other motions can be created by the fluid-structure interaction (FSI) based on the flexibilities of the wings [4-9]. The only prototype of FWNAV that creates enough lift to lift-off is the one presented in Ref. [1]. However, its fabrication includes complicated process, which might make the further miniaturization difficult [10]. The only prototype of FWNAV that is fabricated using the microfabrication process consisting of only the standard steps such as the deposition, the photolithography, the etching, the curing, and the release is the one presented in Refs. [2, 10]. However, enough stroke angle in the wing's flapping motion is obtained using the resonance, which might make the design based on the FSI-cause of the other wing's motions or the FSI-design [3] difficult. In our previous studies, a millimeter-scale wing-shaped hybrid structures mimicking insect wings using the FSI-design was

proposed [3] and fabricated using a microfabrication [11]. Here, a polymer micromachined transmission from the small translational displacement to the large rotational displacement is newly proposed, fabricated, and tested. It follows from this demonstration that the proposed transmission can give further miniaturization of FWNAVs.

II. Materials and Methods

A. Concept of the Polymer Micromachined FWNAV

Figure 1 conceptualizes the proposed polymer micromachined FWNAV, which consists of the transmission, the supporting frame, the piezoelectric bimorph actuator, and the wings. They are typically included in the main components of flapping wing micro air vehicles [12]. However, their significant difference from the previous studies is that they have complete 2.5-dimensional structures such that they can be fabricated using only the standard microfabrication process consisting of only the standard steps such as the deposition, the photolithography, the curing, and the release. For the construction of the FWNAV, one priority is to obtain the wing's flapping motion with the large stroke angle, since the wing's feathering motion, which is the other main motion of the wing to create the lift force [13], can be caused by the fluid-structure interaction (FSI) based on the flexibilities of the wings [4-7]. Some of other motions observed in the insect flapping wings can also be caused by the FSI based on their flexibility [8, 9]. The design using this FSI-cause of the wing's motions or the FSI-design [3] will reduce the electromechanical complexity of the flapping device.
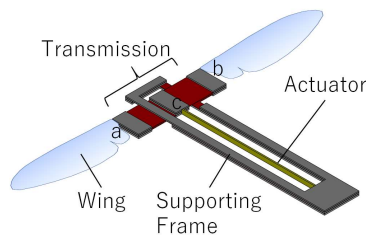

Figure 1. Schematic of the polymer micromachined insect-inspired FWNAV proposed in this study. It consists of the transmission, the supporting frame, the piezoelectric bimorph actuator, and the wings. Their significant difference from the previous studies is that they have 2.5-dimensional structures such that they can be fabricated using only the standard microfabrication steps.

B. Mechanism of the Transmission

Figure 2 shows the transmission mechanism using the large bending of the cantilever plate. Because of the geometrically nonlinear bending, the small translational displacement u_x in the longitudinal axis of the cantilever plate can give the large deflection angle φ at the tip of the

cantilever plate as shown in Figure 2. Different form the previous study [2], the small input can be transmitted to the large output directly using this mechanism.
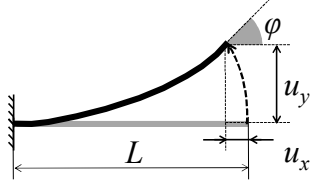

Figure 2. Transmission mechanism using the large bending of the cantilever plate.

C. Basic Design of the Transmission

Figure 3 shows the basic design of the transmission using the mechanism in the previous section. As shown in this figure, the transmission consists of (1) the paralleled elastic hinges, (2) the beams supporting the elastic hinges, (3) the wing attachments, and (4) the actuator attachment. Figure 4 shows the cross-sectional view of this transmission in the xy-plane. The actuator gives the small translational displacement u_x in the point C. This displacement bends the elastic hinges to cause the large rotation φ of the wing attachments based on the mechanism in the previous section. The symmetricity of the two sets of the paralleled elastic hinges about the actuator attachment cancels their reaction moments acting on it.
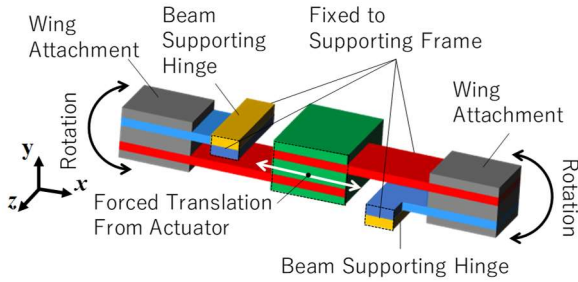

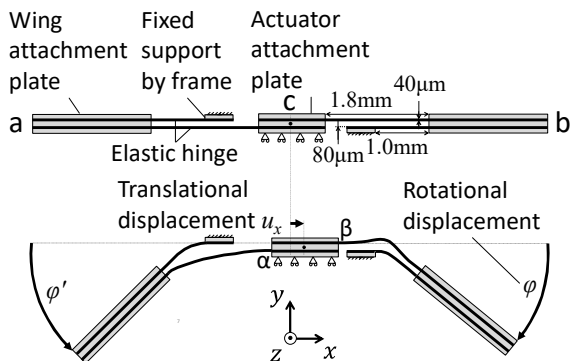Figure 3. Basic design of the transmission.

Figure 4. xy-plane view of the transmission.

D. Detailed Design of the Transmission

Figure 5 shows a detailed design solution of the transmission. The dimensions of the elastic hinge and the supporting beam are shown in Section F. In this figure, the fixed boundary condition is imposed to the supporting frame at the area, where the fixed end of the piezoelectric bimorph actuator is attached, and the transmission and the supporting frame are deformed by the forced displacement $u_x = 170\mu m$. This deformation is calculated using the geometrically nonlinear finite element analysis. Note that u_x is given by the equilibrium between the reaction forces from the transmission and the piezoelectric bimorph actuator (TOKIN Corporation, 20mm length, 3.0mm width, and 0.5mm thickness). The former is given as shown in Figure 6 (solid line) using the geometrically nonlinear finite element analysis, and the latter is given as shown in Figure 6 (dotted line) using the theoretical solutions for the maximum bending displacement δ (no load acting on the actuator) and the maximum reaction force (the blocking force), respectively, as

$$\delta = (3/2)d_{31}(L/t)^2 V , \qquad (1)$$

and

$$F = (2tw/L)Y_{11}d_{31}V , \qquad (2)$$

where d_{31} is the piezoelectric constant, L is the length of the actuator, t is the thickness of the actuator, w is the width of the actuator, V is the applied voltage, and Y_{11} is the Young's modulus. The linear relationship between δ and F is assumed as shown in Figure 6 (dotted line). As shown in Figure 5, the proposed design solution can produce the large flapping angle. This solution produces the maximum magnitude of the flapping angular displacement $\varphi = 21°$ or the stroke angle $\Phi = 42°$, which is comparable with that of actual insects.
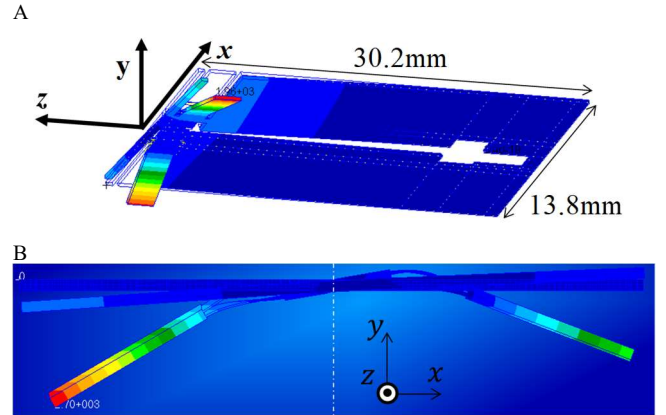

Figure 5. Geometrically nonlinear finite element analysis of transmission. The color contour shows the magnitude of the deformation (A: the bird's eye view, and B: xy-plane view).
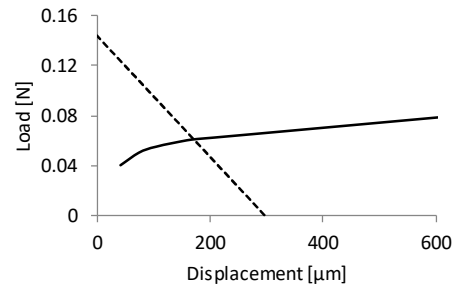

Figure 6. Relationships between the displacement and the reaction force. The solid line indicates that of the transmission given by the nonlinear finite element method, while the dotted line indicates that of the actuator given by the theoretical solutions.

E. Polymer Micromachining Process of the Transmission

Figure 7 shows the microfabrication process of the microstructure with the transmission and the supporting frame using the photosensitive polyimide adhesive sheets. As shown in this figure, the lamination, the exposure, and the development for the sheet are repeated on the substrate, which is made of the Si wafer with the sacrifice layer, until the transmission and the supporting frame are constructed. After those repeated sets of the steps, the transmission and the supporting frame are cured in order to imidize the precursor and to convert it to the polyimide. Finally, the microstructure with the transmission and the supporting frame is released from the substrate.
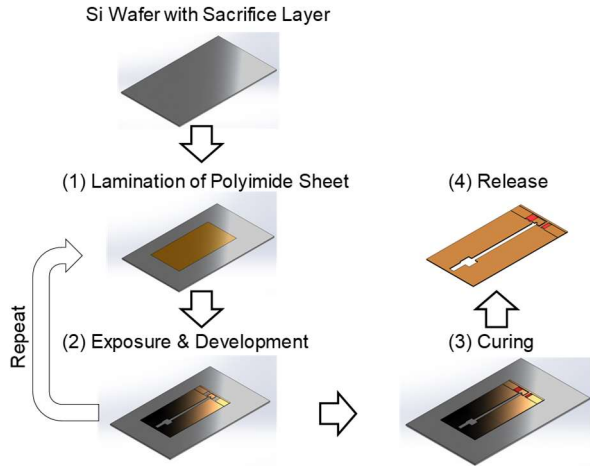

Figure 7. Microfabrication process of the microstructure with the transmission and the supporting frame using the photosensitive polyimide adhesive sheets.

F. Reduction of the Stress in the Polymer Micromachining Process

In the microfabrication steps described above, the various types of the stresses are caused in the polyimide sheets and lead to fracture the elastic hinges. The out-of-plane stress in the lamination steps causes the cracks in the parts of the polyimide sheets forming the hollow structures. The fluid traction force in the development causes the cracks in the elastic hinges. The shrink of the supporting frame due to the curing causes the tension of the beam supporting the elastic hinge, and the tensile stress concentrates in the corner of the boundary between the elastic hinge and the supporting beam to fracture them. The topology, shape, and dimensions of the plane structure of the transmission are designed in order to reduce these stresses. The example is shown in Figure 8, where the stress caused by the shrink of the supporting frame in the curing is considered. In this figure (A), the problem setup of the finite element analysis for the elastic hinge and the supporting beam is shown. The magnitude of the shrink due to the curing is measured from the actual fabrication result, and it is imposed on the boundary between the supporting beam and the supporting frame. The ends of the supporting beam and the elastic hinge are fixed. Figure 8B shows the linear finite element analysis result for the detailed design solution, where the von Mises stress distribution is shown. As shown in this figure, the maximum value of the von Mises stress appears in the corner of the boundary between the elastic hinge and the supporting beam. In order to reduce this stress

such that it is much smaller than the fracture stress, two design parameters shown in Figure 8A (L_t: the length of the supporting beam, R_t: the radius of the corner of the boundary between the elastic hinge and the supporting beam) are parametrically studied. Figure 8C shows the relationship between R_t and the maximum von Mises stress for $L_t = 400\mu m$. As shown in this figure, the optimum values of these design parameters exist.
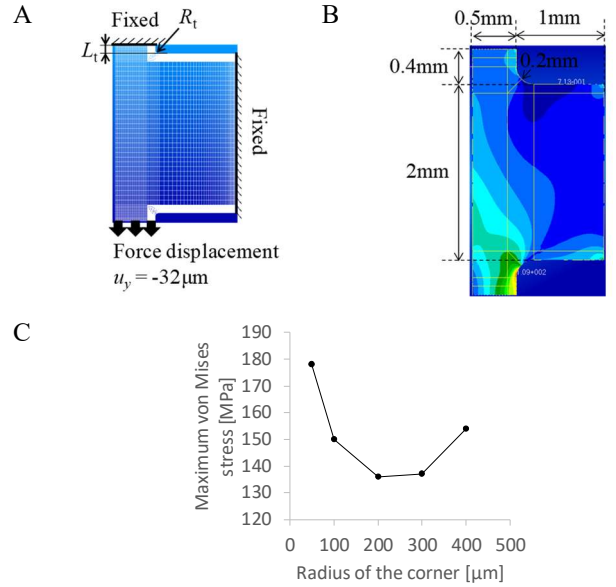

Figure 8. Problem setup of the linear finite element analysis for the elastic hinge and the supporting beam (A), the result of the von Mises stress distribution, which is caused by the shrink of the supporting frame in the curing (B), and the optimum design parameter (C).

III. RESULTS AND DISCUSSION

A. Fabrication of the transmission

Figure 9 shows the transmission and the supporting frame fabricated using the polymer micromachining process, where the photosensitive polyimide adhesive sheets [12] with thickness of 40μm are used. The proposed process consists of only the standard microfabrication steps without any post-assembling. Therefore, the proposed transmission is suitable for the further miniaturization of FWNAVs.
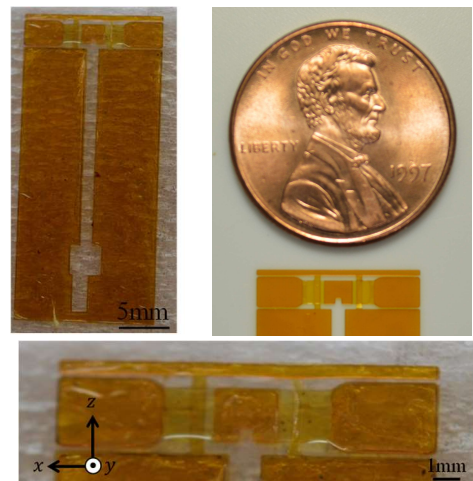

Figure 9. Polymer micromachined transmission and supporting frame using the photosensitive polyimide adhesive sheets.

B. Evaluation of the transmission

Figure 10 shows the experimental apparatus. The supporting frame is fixed using the micro vise, and the forced displacement u_x is imposed on the point where the tip of the piezo bimorph actuator is attached using the micro needle. This displacement is given statically in order to eliminate any dynamic effect. The response of the transmission is shown in Figure 11. This deformation is similar to that obtained using the geometrically nonlinear finite element method in Figure 5B. Figure 12 shows the relationships between u_x and φ, where the black and grey circles indicate the numerical and experimental results, respectively, which are close with each other. As shown in this figure, the transmission can produce the numerically predicted $\Phi = 42°$ as the fabrication accuracy increases. It follows from these results that the proposed transmission can produce the flapping angle comparable with that of actual insects from the small translational displacement given by the micro actuator.
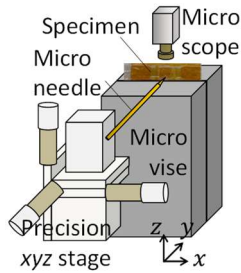

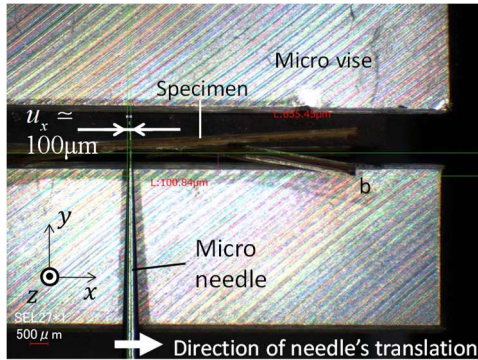Figure 10. Schematic of the experimental apparatus.

Figure 11. Response of the transmission for the translational displacement given by a micro needle.
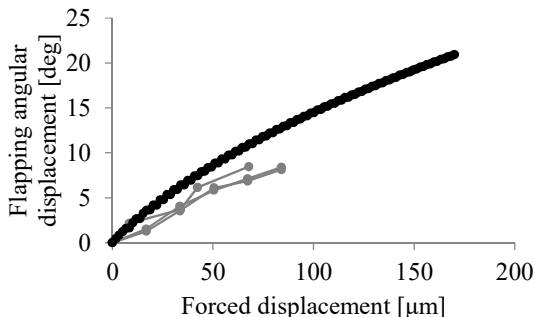

Figure 12. Comparison of experimental and numerical results.

IV. CONCLUSION

This paper presented the polymer micromachined transmission from the small translational displacement given by the micro actuator to the large rotational displacement for further miniaturizing FWNAVs. The proposed transmission used the geometrically nonlinear bending of the cantilever plate as the basic mechanism. The significant difference from the previous studies was that the proposed transmission had the 2.5-dimensional structure. Therefore, it was fabricated using only the standard microfabrication steps without any post-assembling. In this microfabrication, the photosensitive polyimide adhesive sheet was used. The performance of the proposed transmission was evaluated numerically and experimentally. This evaluation demonstrated that the proposed transmission can produce the stroke angle of about 40° without any dynamic effect. It follows from these results that the proposed transmission will contribute the further miniaturization of FWNAVs.

REFERENCES

[1] R. J. Wood, "The first takeoff of a biologically inspired at-scale robotic insect", *IEEE Transactions on Robotics*, 24, 341-347, 2008.
[2] A. Bontemps, et al., "Design and performance of an insect-inspired nano air vehicle", *Smart Materials and Structures*, 22, 014008, 2013.
[3] D. Ishihara, et al., "Fluid-structure interaction design of insect-like micro flapping wing", *Proceedings of VII International Conference on Computational Methods for Coupled Problems in Science and Engineering*, 870-875, 2017.
[4] D. Ishihara and T. Horie, "Fluid-structural interaction modeling of insect flight", *Transactions of the Japan Society of Mechanical Engineers B*, 72 (718), 1410-1417, 2006.
[5] D. Ishihara, et al., "A two-dimensional computational study on the fluid–structure interaction cause of wing pitch changes in dipteran flapping flight", *The Journal of Experimental Biology*, 212, 1-10, 2009.
[6] D. Ishihara, et al., "Passive maintenance of high angle of attack and its lift generation during flapping translation in crane fly wing", *The Journal of Experimental Biology*, 212, 3882-3891, 2009.
[7] D. Ishihara, et al., "An experimental and threedimensional computational study on the aerodynamic contribution to the passive pitching motion of flapping wings in hovering flies", *Bioinspiration and Biomimetics*, 9, 046009, 2014.
[8] D. Ishihara and T. Horie, "Passive mechanism of pitch recoil in flapping insect wings", *Bioinspiration and Biomimetics*, 12, 016008, 2017.
[9] D. Ishihara, "Role of fluid-structure interaction in generating the characteristic tip path of a flapping flexible wing", *Physical Review E*, 98 (3), 032411, 2018.
[10] T. Dargent, et al., "Micromachining of an SU-8 flapping- wing flying micro-electro-mechanical system", *Journal of Micromechanics and Microengineering*, 19, 085028, 2009.
[11] S. Murakami, et al., "Microfabrication of hybrid structure composed of rigid silicon and flexible PI membranes", *Micro & Nano Letters*, 12, 913-915, 2017.
[12] C. Zhang and C. Rossi, "A review of compliant transmission mechanisms for bio-inspired flapping-wing micro air vehicles", *Bioinspiration and Biomimetics*, 12, 025005, 2017.
[13] M. H. Dickinson, et al., Wing rotation and the aerodynamic basis of insect flight, Science, 284, 1954–1960, 1999.
[14] https://www.toray.jp/electronic/semicon/poly/index.html